

# Contributions to Power Extraction in a Dual Oscillating Foil System

Bernardo Luiz R. Ribeiro\* and Jennifer A. Franck†  
*University of Wisconsin-Madison, Madison, WI, 53706*

Oscillating foil turbines can be utilized to extract hydrokinetic energy from tidal or river flows. When foils are placed in arrays, the reduced velocity between foils and the unsteady disturbances associated with the leading foil motion both affect the performance of downstream foils. To compare the performance between foils, a wide range of kinematics is numerically explored in a two-foil tandem configuration with matching strokes, but varying the inter-foil phase angle and spacing. The effects of the wake on the trailing foil performance are quantified by evaluating the difference between the normalized power extracted by each foil. The difference in normalized power extraction is a function of the wake phase parameter,  $\Phi$ , and ranges from -65% to +6%, depending on the kinematic regime. It is also determined that the difference in normalized power is dominated by the pressure contribution from the heave stroke, whereas the viscous components are negligible. In general, these differences illustrate the unsteady effects within the wake of the first foil, and the various interaction modes of the downstream foil. These trends can be used to estimate power in other array configurations and provide a more robust model for wake-foil interactions for energy harvesting.

## I. Introduction

This paper investigates the contributions to power generation in a two-foil energy harvesting system. Oscillating foil turbines can be utilized to extract hydrokinetic energy from tidal or river flows, offering many advantages over rotational turbines, such as operation in shallow waters and lower cut-in speeds. Energy extraction is dependent on the kinematics of the foil, namely operating frequency, pitch and heave amplitude. Thus, performance optimization can be achieved by changing foil kinematics without updating the size and profile of the hydrofoil. Unlike a conventional horizontal-axis turbine, the wake produced by an oscillating foil contains a nearly two-dimensional structured pattern of shed vortices that is directly correlated with the foil kinematics. As the unsteady vortices convect downstream, they can significantly impact performance of bodies placed in the wake, such as downstream foils in arrays. This work quantifies the power components involved in oscillating foils and how they are modified by the presence of an unsteady wake.

In an oscillating foil, power is generated by heave and pitch components, which are a function of the foil kinematics, namely the oscillating frequency, heave and pitch amplitude [1–4]. Heave power is produced when a foil heaves vertically with a positive angle of attack during upstroke, which produces a net positive lifting force and power when multiplied by the heave velocity. The foil reaches the top of the stroke then reverses pitch to a negative angle of attack during downstroke, where the negative lift and velocity vector combine for positive heave power. Pitch power is produced during pitch reversal due to the foil's torque and angular velocity. During the foil stroke, power can be augmented by the formation and shedding of a coherent leading edge vortex (LEV) as the associated low pressure region may cause an increase in lift force. This power increase during the foil stroke occurs if the foil kinematics provides an appropriate time for a vortex to be formed over a foil.

The vortices shed from foils create a coherent structured wake pattern that is correlated with foil kinematics and significantly influences foil-array performance. When a tandem array configuration and the same flapping kinematics for both foils are considered, two parameters dictate the parameter space, the inter-foil phase and the inter-foil spacing. The inter-foil phase describes how one foil is oscillating with respect to the other. Numerical and experimental work show these two parameters greatly affect array performance due to the different wake-foil interactions [5–15].

In a two-turbine array, the power available is different between leading and trailing devices due to the reduced velocity downstream of the lead turbine. This is analyzed by Newman with double actuator-disk theory for vertical-axis wind turbines [16], which is an extension from the traditional single actuator-disk theory developed by Betz [17]. By assuming the flow around the devices is steady, incompressible and inviscid, Newman found an optimal reduced flow velocity downstream of the leading device caused by the blockage and power extraction. Unlike the potential flow analysis of Newman and Betz, the unsteady components of the wake can also be captured by downstream turbines,

---

\*Graduate Research Assistant, Engineering Physics, AIAA Student Member.

†Assistant Professor, Engineering Physics, AIAA Senior Member.

improving the energy extraction potential [18]. Taking inspiration from both these methods, the proposed analysis to evaluate the energy extraction of the trailing foil decomposes the wake into a mean velocity field and a fluctuating or unsteady component. Using this methodology one can separate the effects of each, and identify the major contributions to power extraction.

This paper investigates the difference of power generation between two tandem oscillating foils under various foil kinematics and array parameters, and in doing so, isolates the effects from the unsteady wake. The two power profiles are compared and analyzed in terms of the heave and pitch power while also quantifying the contributions from the pressure and viscous forces. The resulting analysis of separating the various contributions to power generation within an unsteady wake will provide input to wake-foil interaction models for energy harvesting.

## II. Computational Methods

The two-foil array numerical simulations computationally solve the incompressible Navier-Stokes equations,

$$\rho \left( \frac{\partial \mathbf{u}}{\partial t} + \mathbf{u} \cdot \nabla \mathbf{u} \right) + \nabla p = \nabla \cdot \mu \left( \nabla \mathbf{u} + \nabla \mathbf{u}^T \right) \quad (1)$$

$$\nabla \cdot \mathbf{u} = 0 \quad (2)$$

where  $\mathbf{u}$  is the velocity vector,  $p$  is the pressure,  $\rho$  is the fluid's density, and  $\mu$  is the fluid's dynamic viscosity. All numerical simulations are performed at Reynolds number  $Re = 1000$  using a second-order accurate finite volume, pressure-implicit split-operator (PISO) method implemented in *OpenFOAM* [19]. A 2D unstructured mesh is utilized and a full detailed mesh analysis is presented in Ribeiro et al. [15].

Both foils have an elliptical cross-section 10% thick and the prescribed kinematic motion of the foil is described as

$$h(t) = h_o \cos(2\pi f t + \psi) \quad (3)$$

and

$$\theta(t) = \theta_o \cos(2\pi f t + \pi/2 + \psi) \quad (4)$$

where  $h(t)$  and  $\theta(t)$  are the prescribed heave and pitch kinematics, respectively, with a pitching motion about the midpoint of the chord. The frequency of oscillation  $f$ , heave amplitude  $h_o$  and pitch amplitude  $\theta_o$  are the parameters that control the foil motion. Both foils have the same kinematics and the inter-foil phase,  $\psi$ , is zero for the leading foil.

The in-line two-foil array schematic in Figure 1 highlights the foil kinematics, the inter-foil spacing,  $S_x$  and swept area,  $Y_p$ . Since the oncoming flow velocity is different for foil 1 (leading foil) and foil 2 (trailing foil) due to wake deficit, a mean wake velocity,  $\bar{u}_w$ , is defined as

$$\bar{u}_w = 1 - \frac{1}{2Y_p} \int_{-Y_p}^{+Y_p} 1 - \bar{u}(1, y) dy, \quad (5)$$

where the bar ( $\bar{\cdot}$ ) represents a time-averaged quantity and  $1 - \bar{u}(1, y)$  corresponds to the streamwise wake deficit calculated at  $x/c = 1$  as highlighted by a dashed line in Figure 1. The quantity  $2Y_p$  corresponds to the wake width.

To establish the relationship between the trailing foil under different configurations and the wake, Dumas et al. [11] defined a phase shift between the trailing foil motion and the wake from the leading foil assuming it is convecting with the freestream velocity. Updating their definition using the mean wake velocity rather than  $U_\infty$ , the wake phase,  $\Phi$ , is defined by

$$\Phi = 2\pi \frac{S_x}{\bar{u}_w} f^* + \psi, \quad (6)$$

where  $f^* = fc/U_\infty$ . More details on the definitions of  $\bar{u}_w$  and  $\Phi$  are found in Ribeiro et al. [15].

Since heave and pitch are updated simultaneously, a time-varying relative angle of attack with respect to the oncoming flow velocity is generated, which for the leading foil is given by

$$\alpha_{rel}(t) = \tan^{-1} \left( \frac{-\dot{h}(t)}{U_\infty} \right) + \theta(t), \quad (7)$$

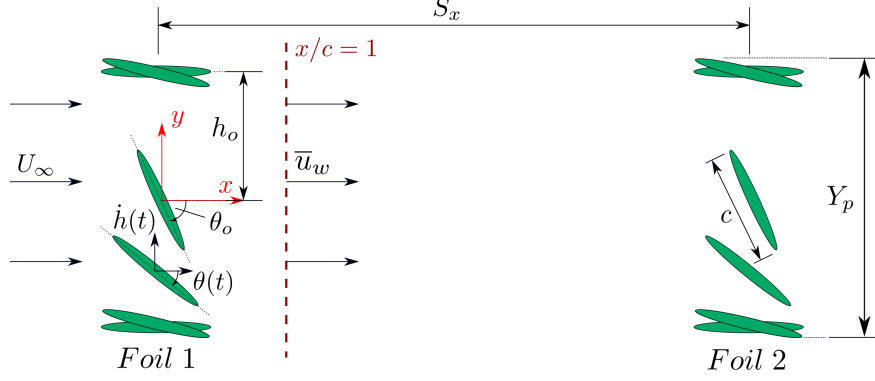


**Fig. 1 In-line foil-array schematic highlighting foil kinematics, inter-foil spacing and swept area,  $Y_p$ .**

with the heave velocity  $\dot{h}(t)$ . A representative relative angle of attack is evaluated when the foil reaches mid-stroke ( $t/T = 0.25$ ) and is labeled as  $\alpha_{T/4}$  (reported here in radians). This is the position where leading foil achieves maximum heave velocity and maximum pitch ( $\theta_o$ ).

### III. Foil Kinematics and Performance Metrics

To evaluate foil performance, the total extracted power is defined by the sum of heave and pitch power

$$P(t) = \underbrace{L(t)\dot{h}(t)}_{\text{heave power}} + \underbrace{T(t)\dot{\theta}(t)}_{\text{pitch power}}, \quad (8)$$

where  $L$  and  $T$  are the lift force and torque on the foil respectively.

To nondimensionalize  $P(t)$ , total power is divided by the energy of the oncoming flow normalized by foil's chord length. For foil 1, this quantity is  $\frac{1}{2}\rho U_\infty^3 c$ . For foil 2, rather than  $U_\infty$ , the mean wake velocity is utilized ( $\frac{1}{2}\rho \bar{u}_w^3 c$ ). Therefore, the nondimensional power or power coefficient,  $C_p(t)$ , is given by

$$C_p(t) = \frac{P_1(t)}{\frac{1}{2}\rho U_\infty^3 c} = \underbrace{C_{h,o}(t) + C_{h,v}(t)}_{\text{heave power}} + \underbrace{C_{\theta,o}(t) + C_{\theta,v}(t)}_{\text{pitch power}}, \quad (9)$$

for foil 1 and

$$C'_p(\Phi, t) = \frac{P_2(\Phi, t)}{\frac{1}{2}\rho \bar{u}_w^3 c} = \underbrace{C'_{h,o}(\Phi, t) + C'_{h,v}(\Phi, t)}_{\text{heave power}} + \underbrace{C'_{\theta,o}(\Phi, t) + C'_{\theta,v}(\Phi, t)}_{\text{pitch power}}, \quad (10)$$

for foil 2, where the subscripts  $h$  and  $\theta$  represent the heave and pitch power and  $o$  and  $v$  correspond to the pressure and viscous components, respectively.

Normalizing power by incorporating mean wake velocity enables a more direct comparison between the energy harvested by foil 1 and foil 2. This comparison can be quantified by the difference in performance between both foils

$$\Delta C_p(\Phi, t) = C'_p(\Phi, t) - C_p(t), \quad (11)$$

and its time-average over a cycle

$$\overline{\Delta C_p}(\Phi) = \frac{1}{T} \int_0^T \Delta C_p(\Phi, t) dt. \quad (12)$$

A similar procedure is done for each component of the foil power. Thus, the time-averaged trailing foil performance can be modeled by five terms

$$\overline{C'_p}(\Phi) = \overline{C_p} + \overline{\Delta C_{h,o}}(\Phi) + \overline{\Delta C_{h,v}}(\Phi) + \overline{\Delta C_{\theta,o}}(\Phi) + \overline{\Delta C_{\theta,v}}(\Phi). \quad (13)$$

The re-normalization of the second foil's power coefficient accounts for the reduced velocity available in the wake, due to the presence of the first foil, in a mean sense. Thus, the difference between the two power curves, or the quantity  $\Delta C_p$ , represents the effects on the trailing foil performance due to the unsteadiness within the wake between the two foils. Due to the timing of the unsteady wake-foil interactions,  $\overline{\Delta C_p}$  is strongly dependent on  $\Phi$ , the wake phase parameter, and can also be tracked throughout the cycle as a function of time,  $t$ .

The foil kinematics, the inter-foil spacing, and the mean wake velocities are outlined in Table 1. The  $\alpha_{T/4}$  values correspond to the leading foil (Equation 7) and for simplicity, the same value is used for the trailing foil, although the effective  $\alpha_{T/4}$  on the trailing foil is reduced due to the lower effective velocity. Each kinematics is explored at 12 inter-foil phases sampled at every  $30^\circ$  from  $0^\circ$  to  $330^\circ$ . Frequency and heave amplitude are nondimensionalized by  $U_\infty$  and  $c$  in the following equations as  $f^* = fc/U_\infty$  and  $h_o^* = h_o/c$ . Reduced frequency, pitch amplitude and heave amplitude are varied from  $f^* = 0.10 - 0.15$ ,  $\theta_o = 55^\circ - 75^\circ$ ,  $h_o^* = 0.75 - 1.50$ .

**Table 1 Kinematics and array configurations with their respective  $\alpha_{T/4}$ , inter-foil spacing,  $S_x$ , and mean wake velocity,  $\bar{u}_w$ . Markers used in Figure 4 are shown.**

Marker	Kinematics	$\alpha_{T/4}$	$S_x$	$\bar{u}_w$
	$f^* = 0.12; h_o^* = 1.50; \theta_o = 55^\circ$	0.11	6	0.98
	$f^* = 0.17; h_o^* = 1.00; \theta_o = 55^\circ$	0.14	6	0.96
	$f^* = 0.16; h_o^* = 1.00; \theta_o = 55^\circ$	0.17	6	0.95
	$f^* = 0.15; h_o^* = 1.00; \theta_o = 55^\circ$	0.20	6	0.95
	$f^* = 0.15; h_o^* = 1.25; \theta_o = 65^\circ$	0.27	6	0.93
	$f^* = 0.12; h_o^* = 1.00; \theta_o = 55^\circ$	0.31	6	0.92
	$f^* = 0.12; h_o^* = 1.25; \theta_o = 65^\circ$	0.38	6	0.91
	$f^* = 0.15; h_o^* = 1.00; \theta_o = 65^\circ$	0.38	6	0.90
	$f^* = 0.10; h_o^* = 1.00; \theta_o = 55^\circ$	0.40	6	0.90
	$f^* = 0.14; h_o^* = 1.00; \theta_o = 65^\circ$	0.41	6	0.88
	$f^* = 0.13; h_o^* = 1.00; \theta_o = 65^\circ$	0.45	6	0.88
	$f^* = 0.10; h_o^* = 1.25; \theta_o = 65^\circ$	0.47	6	0.88
	$f^* = 0.12; h_o^* = 1.00; \theta_o = 65^\circ$	0.49	4	0.87
	$f^* = 0.12; h_o^* = 1.00; \theta_o = 65^\circ$	0.49	5	0.87
	$f^* = 0.12; h_o^* = 1.00; \theta_o = 65^\circ$	0.49	6	0.87
	$f^* = 0.15; h_o^* = 0.75; \theta_o = 65^\circ$	0.52	6	0.84
	$f^* = 0.11; h_o^* = 1.00; \theta_o = 65^\circ$	0.53	6	0.86
	$f^* = 0.15; h_o^* = 1.00; \theta_o = 75^\circ$	0.55	6	0.83
	$f^* = 0.10; h_o^* = 1.00; \theta_o = 65^\circ$	0.57	6	0.85
	$f^* = 0.12; h_o^* = 0.75; \theta_o = 65^\circ$	0.62	6	0.81
	$f^* = 0.12; h_o^* = 1.00; \theta_o = 75^\circ$	0.66	6	0.81
	$f^* = 0.10; h_o^* = 0.75; \theta_o = 65^\circ$	0.69	6	0.81
	$f^* = 0.10; h_o^* = 1.00; \theta_o = 75^\circ$	0.75	6	0.82

Three regimes of kinematics are explored, as defined by Ribeiro et al. [15]. Regime I groups the kinematics with  $\alpha_{T/4} = 0.11 - 0.20$ , while regimes II and III, groups kinematics with  $\alpha_{T/4} = 0.27 - 0.49$  and  $\alpha_{T/4} = 0.52 - 0.75$ .

Figure 2a has the time-averaged power coefficient of the leading foil as a function of  $\alpha_{T/4}$ . Figure 2b displays the power coefficient of the trailing foil. Since this is a function of the wake phase,  $\Phi$ , the maximum and minimum values of the time-averaged power coefficient are displayed. The maximum values are very similar to the leading foil performance across  $\alpha_{T/4}$ . A larger variation is found within regime III due to stronger flow separation at high  $\alpha_{T/4}$  values. For some kinematics, the minimum power coefficient is below zero, indicating the second foil does not extract any energy from the flow.

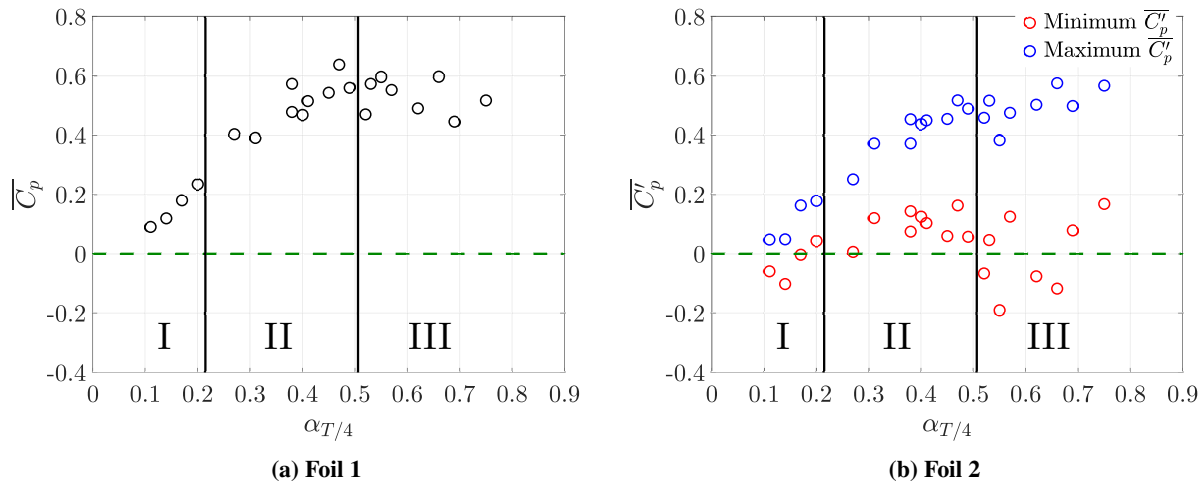


**Fig. 2 Time-averaged power coefficient. For foil 2, the minimum and maximum values with respect to changing wake phase,  $\Phi$ , are shown.**

#### IV. Contributions to Power Generation

To explore the difference in power between foils, the components of  $\overline{\Delta C_p}$  are analyzed for a representative set of kinematics from each regime in Figure 3. For all regimes, the total  $\overline{\Delta C_p}$  values are almost always negative, indicating the trailing foil has a lower performance compared with the leading foil. This is expected in the tandem configuration tested. However, depending on the foil kinematics and wake phase, there are a few configurations where  $\overline{\Delta C_p}$  is approximately zero, indicating that the normalized trailing foil power coefficient matches that of the leading foil.

Each regime shows different  $\overline{\Delta C_p}$  trends with respect to wake phase. Regime I does not show strong variations of  $\overline{\Delta C_p}$  across wake phases as seen by the roughly constant values between  $\Phi = 180^\circ - 350^\circ$ . In contrast, for the case in regime II, there is a clear minimum and maximum located at approximately  $\Phi = 0^\circ$  and  $\Phi = 120^\circ$ , respectively. The kinematics analyzed in regime III has a much stronger  $\overline{\Delta C_p}$  variation for a small change in wake phase as seen at phases  $\Phi > 310^\circ$  and  $\Phi < 70^\circ$  and it shows  $\overline{\Delta C_p}$  close to zero in phase range  $\Phi = 220^\circ - 280^\circ$ .

Each  $\overline{\Delta C_p}$  can be broken into components based on heave, pitch, viscous and pressure contributions. The heave power from pressure forces,  $\overline{\Delta C_{h,o}}$  is the strongest contribution in each of the kinematics tested, accounted for an average of 74% of  $\overline{\Delta C_p}$ , with a standard deviation of 10%. In contrast, the pitch power from pressure forces,  $\overline{\Delta C_{\theta,o}}$ , corresponds to roughly 19% on average, with same standard deviation. The viscous terms are close to zero across all regimes, thus contributing equally to foils 1 and 2. This indicates that the unsteady effects captured by this analysis are primarily due to pressure, and likely a consequence of the low pressure region imposed by vortices in the wake.

Therefore, in the following analysis the  $C_{h,o}$  term is considered to examine the unsteady wake effects on the trailing foil performance.

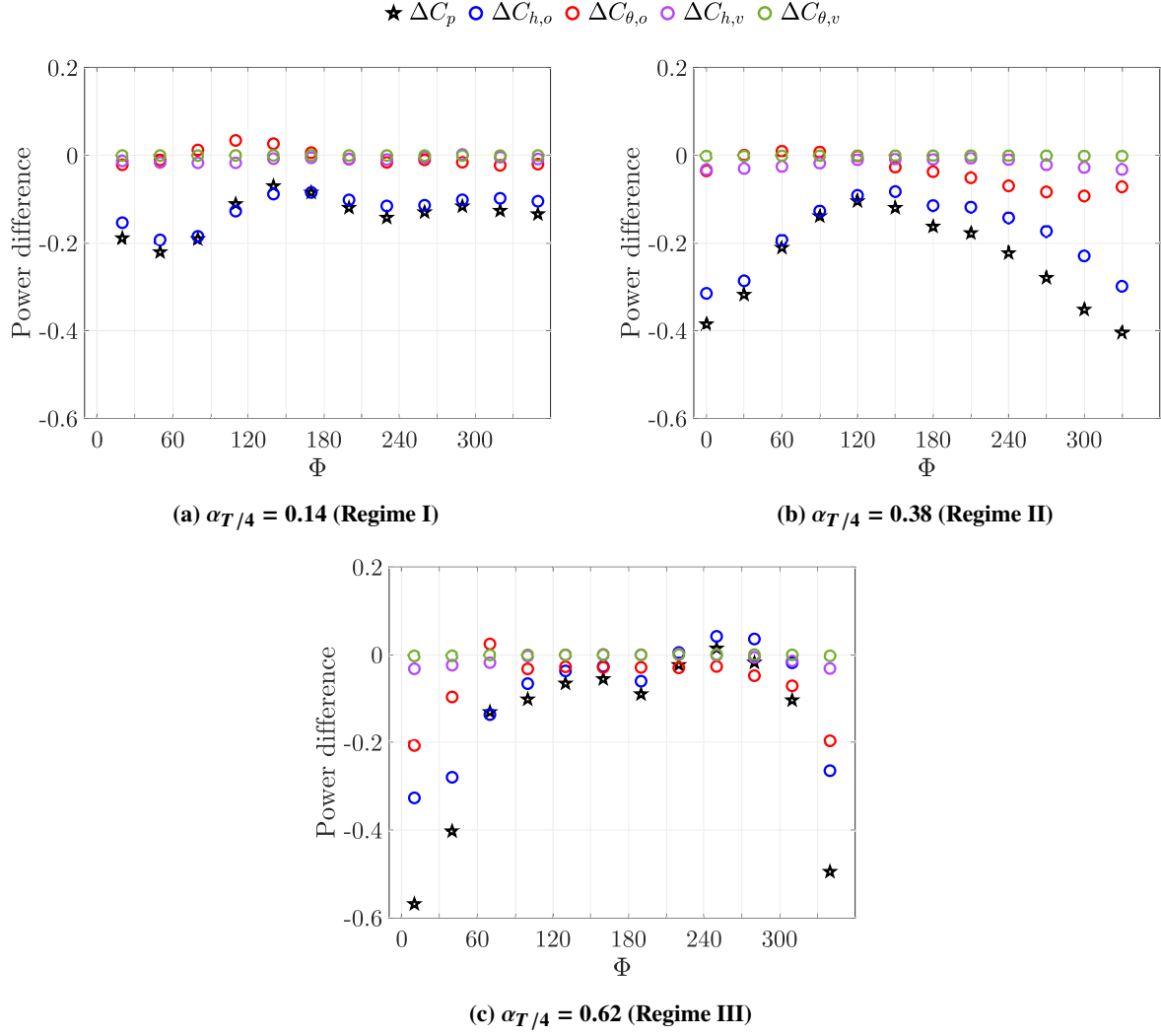


**Fig. 3** Power components of a representative foil kinematics from each regime. For  $\alpha_{T/4} = 0.38$ , the kinematics  $f^* = 0.15$ ;  $h_o^* = 1.00$ ;  $\theta_o = 65^\circ$  is utilized.

In Figure 4, the heave power from pressure,  $\overline{\Delta C_{h,o}}$ , is computed for all configurations. In all three regimes, most trailing foil kinematics display a performance similar to that of the leading foil ( $\overline{\Delta C_{h,o}} \approx 0$ ) when oscillating out-of-phase from the leading foil wake ( $\Phi \approx 180^\circ$ ). As  $\alpha_{T/4}$  increases, there is a stronger dependency on the wake phase as demonstrated by the difference between the maximum and minimum of  $\overline{\Delta C_{h,o}}$  increasing from 0.2 in regime I, to 0.6 in regime III. The trends found in the representative kinematics within each regime are maintained as there is a larger variation of  $\overline{\Delta C_{h,o}}$  in regime III compared with lower  $\alpha_{T/4}$  regimes, especially at phases  $\Phi > 330^\circ$  and  $\Phi < 40^\circ$ . Regime III is thus more dependent on foil kinematics compared to regimes I and II and all foil kinematics simulated in the latter regimes collapse into the same trend.

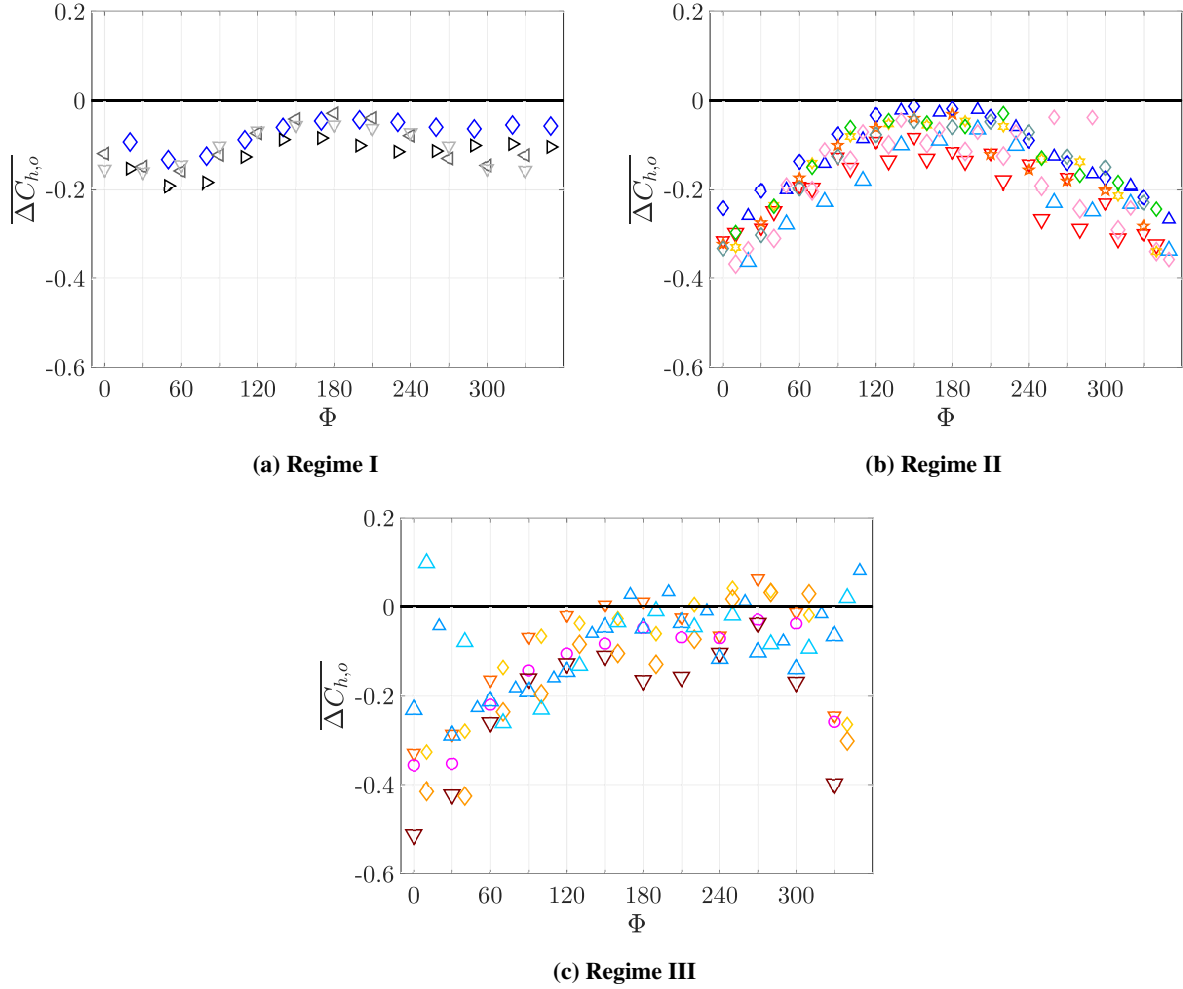


**Fig. 4** Heave power from pressure force,  $\overline{\Delta C_{h,o}}$ .

To investigate the variation of  $C_{h,o}$  throughout time and how it is affected by the foil kinematics, the power from each foil with kinematics  $f^* = 0.12$ ;  $h_o^* = 1.00$ ;  $\theta_o = 55^\circ$  ( $\alpha_{T/4} = 0.31$ ) at three different wake phases are analyzed in Figure 5. The selected wake phases cover cases where the trailing foil performed similarly to the leading foil on average ( $\Phi = 150^\circ$ ) to where the largest performance difference between foils is found ( $\Phi = 0^\circ$ ). Green areas represent the times when the power performance of the trailing foil is higher than the leading foil and yellow regions correspond to the opposite. Although the  $\overline{\Delta C_{h,o}}$  value for the phase  $\Phi = 150^\circ$  is approximately zero, the  $C_{h,o}$  profile of the foil 2 does not follow foil 1. This means that the green and yellow areas are approximately the same, and thus the integral of the power difference with respect to time is close to zero.

To physically explain the power difference between foils, the bottom row of Figure 5 displays the vorticity flow fields at different wake phases when the trailing foil is at  $t/T = 0.20$  (see black circles in Figure 5). At  $\Phi = 150^\circ$ , foil 2 avoids strong interactions with the oncoming wake structures as it is oscillating out-of-phase and thus the wake unsteadiness does not significantly impact trailing foil performance. For cases where foil 2 is more closely following the leading foil wake ( $\Phi \approx 0^\circ$ ), stronger wake-foil interactions are expected as there is a direct impingement of the oncoming vortices on the trailing foil as illustrated by the sharp drop of  $C_{h,o}$  for foil 2 at  $t/T = 0.40$ .

For foil kinematics with higher  $\alpha_{T/4}$  ( $\alpha_{T/4} = 0.66$ ), the same analysis is displayed in Figure 6. At  $\Phi = 250^\circ$ , although there is a large power difference between foils with respect to time, the  $\overline{\Delta C_{h,o}}$  is approximately zero, emphasizing that a negligible power difference does not necessarily correspond to the absence of unsteady wake effects on trailing foil performance. For the phase  $\Phi = 100^\circ$ , the direct impingement of the leading edge vortex from the leading foil onto the trailing foil diminishes its performance as shown by the  $\Delta C_{h,o} \approx 0.6$  between foils. Similarly from the foil

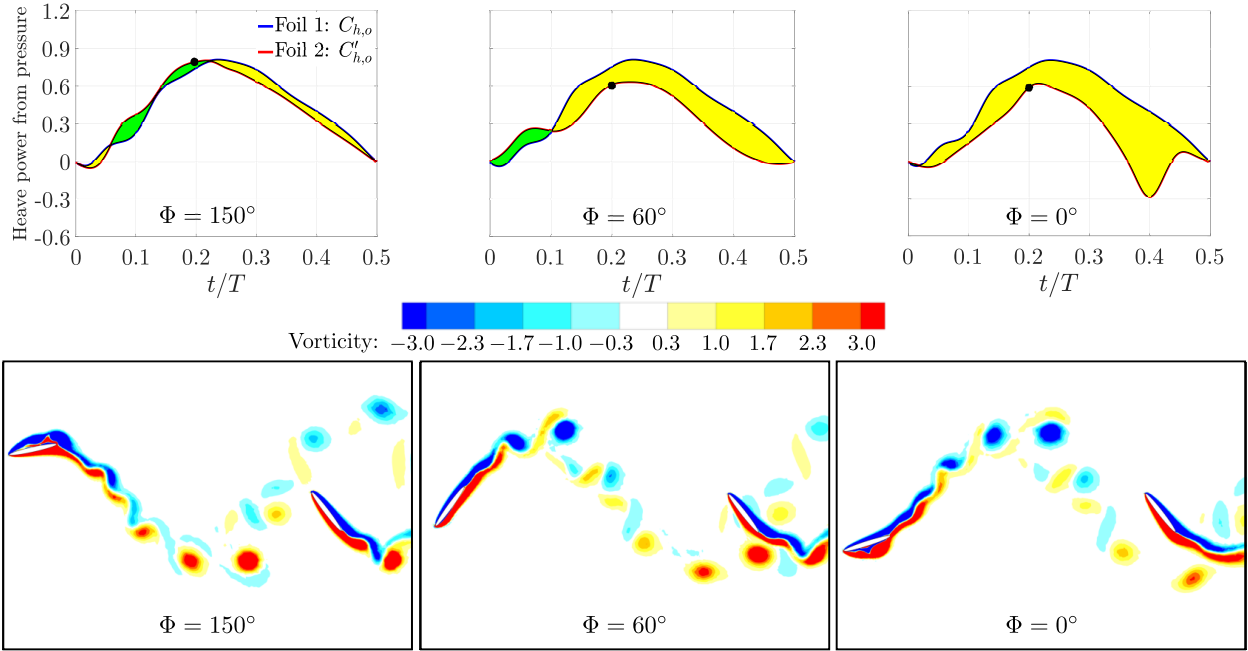


**Fig. 5** Power component  $C_{h,o}$  and  $C'_{h,o}$  for the foil kinematics  $f^* = 0.12$ ;  $h_o^* = 1.00$ ;  $\theta_o = 55^\circ$  ( $\alpha_{T/4} = 0.31$ ) at three different wake phases. The bottom row displays the instantaneous vorticity flow fields at times represented by the black circles ( $t/T = 0.20$ ).

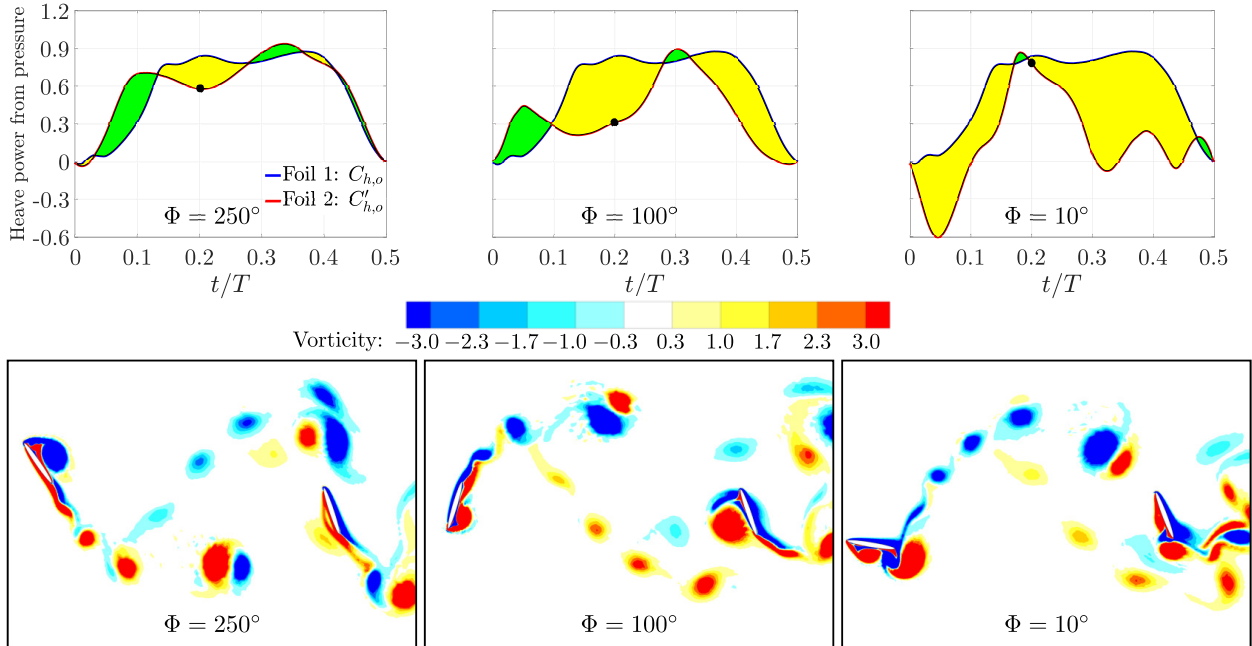


**Fig. 6** Power component  $C_{h,o}$  and  $C'_{h,o}$  for the foil kinematics  $f^* = 0.12$ ;  $h_o^* = 1.00$ ;  $\theta_o = 75^\circ$  ( $\alpha_{T/4} = 0.66$ ) at three different wake phases. The bottom row displays the instantaneous vorticity flow fields at times represented by the black circles ( $t/T = 0.20$ ).

kinematics with lower  $\alpha_{T/4}$ , when the trailing foil motion is more closely synchronized with the leading foil's wake, the largest performance gap between foils is found. In contrast, for phase  $\Phi = 10^\circ$  at  $t/T = 0.20$ , the wake-foil interaction momentarily increases trailing foil performance. The interaction of opposite sign vortices close to the trailing edge of the trailing foil increases the pressure at the bottom surface, which then increases the pressure gradient and power generation. For later times than  $t/T = 0.20$ , the trailing foil performance is greatly affected by the wake structures as seen by the higher power variation throughout time compared with other wake phases and lower  $\alpha_{T/4}$  values.

## V. Conclusion

This paper quantifies the contributions to power generation of an oscillating foil when it is operating within the unsteady wake of another foil. This tandem configuration is governed by the spacing between the two foils, but also its inter-foil phase angle, and assumes that both foils have the same kinematic stroke.

The mean streamwise velocity between the two foils is utilized to normalize the power extraction of the second foil, and provide a direct comparison with the power extraction of the lead foil. In this manner, the difference between the two power curves represents the unsteady contributions to the power extraction. For most scenarios in the tandem configuration, the power extraction difference,  $\Delta C_p$  is negative, meaning that the unsteady wake interactions lower the relative power extraction with respect to the lead foil.

However, there are some scenarios when the trailing foil has similar performance to the leading foil, or a  $\overline{\Delta C_p} \approx 0$ . This is when the oscillation is out-of-phase with the wake, and the trailing foil avoids direct interactions with wake vortices.

The difference in power is split into components in terms of heave/pitch contributions, and pressure/viscous contributions. The heave power from pressure forces is the most dominant term as it follows the same trends and approximately same magnitude as the total power difference.

Finally, the difference in power follows a different trend for three regimes of power extraction. Regime I, for low relative angles of attack, has little variation with respect to wake phase angle. Regime II, a moderate angle of attack, demonstrates a strong sinusoidal collapse with respect to wake phase. In Regime III, a higher power variation is observed for due to the high relative angles of attack ( $\alpha_{T/4} > 0.49$ ). This is evidence of stronger vortex-foil interactions compared with lower angles of attack.

## VI. Acknowledgments

This material is based upon work supported by the National Science Foundation under award CBET-1921594. This research was conducted using computational resources and services at the Center for Computation and Visualization at Brown University.

## References

- [1] J. Y. Lai, J. C. S., and Platzer, M. F., "A review of progress and challenges in flapping foil power generation," *Progress in Aerospace Sciences*, Vol. 67, 2014. doi:10.1016/j.paerosci.2013.11.001.
- [2] Xiao, Q., and Zhu, Q., "A review on flow energy harvesters based on flapping foils," *Journal of Fluids and Structures*, Vol. 46, 2014. doi:10.1016/j.jfluidstructs.2014.01.002.
- [3] Wu, X., Zhang, X., Tian, X., Li, X., and Lu, W., "A review on fluid dynamics of flapping foils," *Ocean Engineering*, Vol. 195, 2020. doi:10.1016/j.oceaneng.2019.106712.
- [4] Laws, N. D., and Epps, B. P., "Hydrokinetic energy conversion: Technology, research, and outlook," *Renewable and Sustainable Energy Reviews*, Vol. 57, 2016. doi:10.1016/j.rser.2015.12.189.
- [5] Platzer, M., Ashraf, M., Young, J., and Lai, J., "Development of a New Oscillating-Wing Wind and Hydropower Generator," *47th AIAA Aerospace Sciences Meeting including The New Horizons Forum and Aerospace Exposition*, American Institute of Aeronautics and Astronautics, 2009. doi:10.2514/6.2009-1211.
- [6] Ashraf, M. A., Young, J., Lai, J. C. S., and Platzer, M. F., "Numerical analysis of an oscillating-wing wind and hydropower generator," *AIAA Journal*, Vol. 49, 2011. doi:10.2514/1.J050577.
- [7] Broering, T. M., and Lian, Y.-S., "The effect of phase angle and wing spacing on tandem flapping wings," *Acta Mechanica Sinica*, Vol. 28, 2012. doi:10.1007/s10409-012-0210-8.

- [8] Broering, T. M., Lian, Y.-S., and Henshaw, W., “Numerical Investigation of Energy Extraction in a Tandem Flapping Wing Configuration,” *AIAA Journal*, Vol. 50, 2012. doi:10.2514/1.J051104.
- [9] Karakas, F., and Fenercioglu, I., “Effect of phase angle on tandem flapping-wing power generation,” *International Journal of Energy Production and Management*, Vol. 2, 2017. doi:10.2495/EQ-V2-N1-95-105.
- [10] Ma, P., Wang, Y., Xie, Y., Han, J., Sun, G., and Zhang, J., “Effect of wake interaction on the response of two tandem oscillating hydrofoils,” *Energy Science & Engineering*, Vol. 7, 2019. doi:10.1002/ese3.286.
- [11] Kinsey, T., and Dumas, G., “Optimal tandem configuration for oscillating-foils hydrokinetic turbine,” *Journal of Fluids Engineering*, Vol. 134, 2012. doi:10.1115/1.4005423.
- [12] Kinsey, T., Dumas, G., Lalande, G., Ruel, J., Méhut, A., Viarouge, P., Lemay, J., and Jean, Y., “Prototype testing of a hydrokinetic turbine based on oscillating hydrofoils,” *Renewable Energy*, Vol. 36, 2011. doi:10.1016/j.renene.2010.11.037.
- [13] Xu, J., Sun, H., and Tan, S., “Wake vortex interaction effects on energy extraction performance of tandem oscillating hydrofoils,” *Journal of Mechanical Science and Technology*, Vol. 30, 2016. doi:10.1007/s12206-016-0835-9.
- [14] Xu, G., and Xu, W., “Energy extraction of two flapping foils with tandem configurations and vortex interactions,” *Engineering Analysis with Boundary Elements*, Vol. 82, 2017. doi:10.1016/j.enganabound.2017.06.010.
- [15] Ribeiro, B. L. R., Su, Y., Guillaumin, Q., Breuer, K. S., and Franck, J. A., “Wake-foil interactions and energy harvesting efficiency in tandem oscillating foils,” *Phys. Rev. Fluids*, Vol. 6, 2021. doi:10.1103/PhysRevFluids.6.074703.
- [16] Newman, B., “Actuator-disc theory for vertical-axis wind turbines,” *Journal of Wind Engineering and Industrial Aerodynamics*, Vol. 15, 1983. doi:https://doi.org/10.1016/0167-6105(83)90204-0.
- [17] Betz, A., *Windmills in the light of modern research*, Vol. XV, National Advisory committee for aeronautics, 1928. Report No. NACA-TM-474.
- [18] Dabiri, J. O., “Theoretical framework to surpass the Betz limit using unsteady fluid mechanics,” *Physical Review Fluids*, Vol. 5, 2020. doi:10.1103/PhysRevFluids.5.022501.
- [19] Weller, H. G., Tabor, G., Jasak, H., and Fureby, C., “A tensorial approach to computational continuum mechanics using object-oriented techniques,” *Computers in Physics*, Vol. 12, 1998. doi:10.1063/1.168744.